Unidirectional Growth of Microbumps on (111)-Oriented and Nanotwinned Copper

Hsiang-Yao Hsiao *et al.*

Science **336**, 1007 (2012);
DOI: 10.1126/science.1216511

absent when the superconductor is replaced by a normal conductor. Based on these observations, we conclude that our spectroscopy experiment provides evidence for the existence of Majorana fermions.

Improving the electron mobility and optimizing the gate coupling will enable us to map out the phase diagram of the topological superconductor in the plane of E_Z and μ (*27*–*30*). It will be interesting to control the subband occupation underneath the superconductor down to a single subband to make direct comparisons to theoretical models. Currently, we probe induced gaps and states from all occupied subbands, each with a different coupling to the tunnel barrier. The topological state in the topmost subband likely has the weakest coupling to the tunnel barrier. Single-subband models (*8*, *9*) predict that one should observe a closing of the topological gap; however, in multisubband systems, this gap closing may not be visible. The constant gap in Fig. 2 may come from lower subbands. The presence of multiple subbands together with our finite temperature may also be the reason that our ZBP is currently only ~5% of the theoretical zero-temperature limit of $2e^2/h$ (*12*, *14*).

Finally, we note that this work does not address the topological properties of Majorana fermions. The first step toward demonstrating topological protection would be the observation of conductance quantization (*12*, *32*). Second, in a Josephson tunnel junction with phase difference φ and a pair of Majoranas on either side, the current-phase relation becomes proportional to $\sin(\varphi/2)$. The factor 2 is another distinct Majorana signature, which should be observable as an h/e flux periodicity in a superconducting quantum interference device measurement (*8*, *9*). The last type of experiment involves the exchange of Majoranas around each other. Such braiding experiments can reveal their non-Abelian statistics, which are the ultimate proof of topologically protected Majorana fermions (*33*–*35*).

References and Notes

1. E. Majorana, *Soryushiron Kenkyu* (Engl. transl.) **63**, 149 (1981) [translation from *Nuovo Cimento* **14**, 171 (1937)].
2. F. Wilczek, *Nat. Phys.* **5**, 614 (2009).
3. M. Franz, *Physics* **3**, 24 (2010).
4. A. Yu. Kitaev, *Phys. Usp.* **44**, 131 (2001).
5. L. Fu, C. L. Kane, *Phys. Rev. Lett.* **100**, 096407 (2008).
6. J. D. Sau, R. M. Lutchyn, S. Tewari, S. Das Sarma, *Phys. Rev. Lett.* **104**, 040502 (2010).
7. J. Alicea, *Phys. Rev. B* **81**, 125318 (2010).
8. R. M. Lutchyn, J. D. Sau, S. Das Sarma, *Phys. Rev. Lett.* **105**, 077001 (2010).
9. Y. Oreg, G. Refael, F. von Oppen, *Phys. Rev. Lett.* **105**, 177002 (2010).
10. C. W. J. Beenakker, http://arxiv.org/abs/1112.1950 (2011).
11. J. Alicea, http://arxiv.org/abs/1202.1293 (2012).
12. K. T. Law, P. A. Lee, T. K. Ng, *Phys. Rev. Lett.* **103**, 237001 (2009).
13. K. Flensberg, *Phys. Rev. B* **82**, 180516 (2010).
14. J. D. Sau, S. Tewari, R. Lutchyn, T. Stanescu, S. Das Sarma, *Phys. Rev. B* **82**, 214509 (2010).
15. S. R. Plissard *et al.*, *Nano Lett.* **12**, 1794 (2012).
16. H. A. Nilsson *et al.*, *Nano Lett.* **9**, 3151 (2009).
17. S. Nadj-Perge *et al.*, *Phys. Rev. Lett.* **108**, 166801 (2012).
18. P. W. Brouwer, M. Duckheim, A. Romito, F. von Oppen, *Phys. Rev. Lett.* **107**, 196804 (2011).
19. J. D. Sau, S. Tewari, S. Das Sarma, *Phys. Rev. B* **85**, 064512 (2012).
20. See supplementary materials on *Science* Online.
21. J. D. Pillet *et al.*, *Nat. Phys.* **6**, 965 (2010).
22. T. Dirks *et al.*, *Nat. Phys.* **7**, 386 (2011).
23. H. le Sueur, P. Joyez, H. Pothier, C. Urbina, D. Esteve, *Phys. Rev. Lett.* **100**, 197002 (2008).
24. S. Sasaki *et al.*, *Nature* **405**, 764 (2000).
25. M. Zareyan, W. Belzig, Yu. V. Nazarov, *Phys. Rev. B* **65**, 184505 (2002).
26. B. J. van Wees, P. de Vries, P. Magnée, T. M. Klapwijk, *Phys. Rev. Lett.* **69**, 510 (1992).
27. M. Wimmer, A. R. Akhmerov, M. V. Medvedyeva, J. Tworzydło, C. W. Beenakker, *Phys. Rev. Lett.* **105**, 046803 (2010).
28. A. C. Potter, P. A. Lee, *Phys. Rev. Lett.* **105**, 227003 (2010).
29. R. M. Lutchyn, T. D. Stanescu, S. Das Sarma, *Phys. Rev. Lett.* **106**, 127001 (2011).
30. T. D. Stanescu, R. M. Lutchyn, S. Das Sarma, *Phys. Rev. B* **84**, 144522 (2011).
31. P. Středa, P. Šeba, *Phys. Rev. Lett.* **90**, 256601 (2003).
32. M. Wimmer, A. R. Akhmerov, J. P. Dahlhaus, C. W. J. Beenakker, *N. J. Phys.* **13**, 053016 (2011).
33. N. Read, D. Green, *Phys. Rev. B* **61**, 10267 (2000).
34. D. A. Ivanov, *Phys. Rev. Lett.* **86**, 268 (2001).
35. C. Nayak, S. H. Simon, A. Stern, M. Freedman, S. Das Sarma, *Rev. Mod. Phys.* **80**, 1083 (2008).

Acknowledgments: We thank D. Thoen and T. Klapwijk for sharing their NbTiN technology and A. Akhmerov, J. Alicea, C. Beenakker, M. Freedman, F. Hassler, G. Immink, H. Keïjzers, C. Marcus, S. Nadj-Perge, Y. Nazarov, I. van Weperen, M. Wimmer, and D. van Woerkom for discussions and assistance. This work has been supported by European Research Council, Netherlands Organization for Scientific Research (NWO), Foundation for Fundamental Research on Matter (FOM), and Microsoft Corporation Station Q.

Supplementary Materials

www.sciencemag.org/cgi/content/full/science.1222360/DC1
Supplementary Text
Figs. S1 to S14
References (*36*, *37*)
Data Files

23 March 2012; accepted 5 April 2012
Published online 12 April 2012;
10.1126/science.1222360

Unidirectional Growth of Microbumps on (111)-Oriented and Nanotwinned Copper

Hsiang-Yao Hsiao,[1] Chien-Min Liu,[1] Han-wen Lin,[1] Tao-Chi Liu,[1] Chia-Ling Lu,[1] Yi-Sa Huang,[1] Chih Chen,[1]* K. N. Tu[2]*

Highly oriented [111] Cu grains with densely packed nanotwins have been fabricated by direct-current electroplating with a high stirring rate. The [111]-oriented and nanotwinned Cu (nt-Cu) allow for the unidirectional growth of Cu_6Sn_5 intermetallics in the microbumps of three-dimensional integrated-circuit packaging; a uniform microstructure in a large number of microbumps of controlled orientation can be obtained. The high-density twin boundaries in the nt-Cu serve as vacancy sinks during the solid-state reaction between Pb-free solder and Cu and greatly reduce the formation of Kirkendall (or Frenkel) voids.

A change from two-dimensional to three-dimensional integrated circuits (3D IC) is under way in the microelectronics industry as the limits of very-large-scale integration in silicon chip technology are approached (*1*). In essence, 3D IC is intended to bring packaging technology and chip technology together. With respect to scaling the density of solder bumps on a chip surface, the diameter of a flip-chip solder bump is about 100 μm today, and it should be possible to reduce this to 1 μm. This improvement will increase the density of bumps per unit area by 4 orders of magnitude, yet the solder volume will be reduced by 6 orders of magnitude. However, the melting point of the solder remains unchanged, meaning that each microbump may contain only a few grains after processing. Variation in the grain orientation may lead to a wide distribution of the orientation-dependent properties of microbumps, which may in turn lead to early failure and low reliability. This is because certain grain orientations allow fast diffusion and electromigration (*2*, *3*). Because there are a large number of microbumps on a stack of chips in a 3D IC, achieving a uniform microstructure in several thousand of these microbumps on each chip is a critical issue.

Maintaining control over the microstructure of the microbumps is nontrivial because of

[1]Department of Materials Science and Engineering, National Chiao Tung University, Hsinchu, Taiwan 30010, Republic of China. [2]Department of Materials Science and Engineering, University of California at Los Angeles, Los Angeles, CA 90095, USA.

*To whom correspondence should be addressed. E-mail: chih@mail.nctu.edu.tw (C.C.); kntu@ucla.edu (K.N.T.)

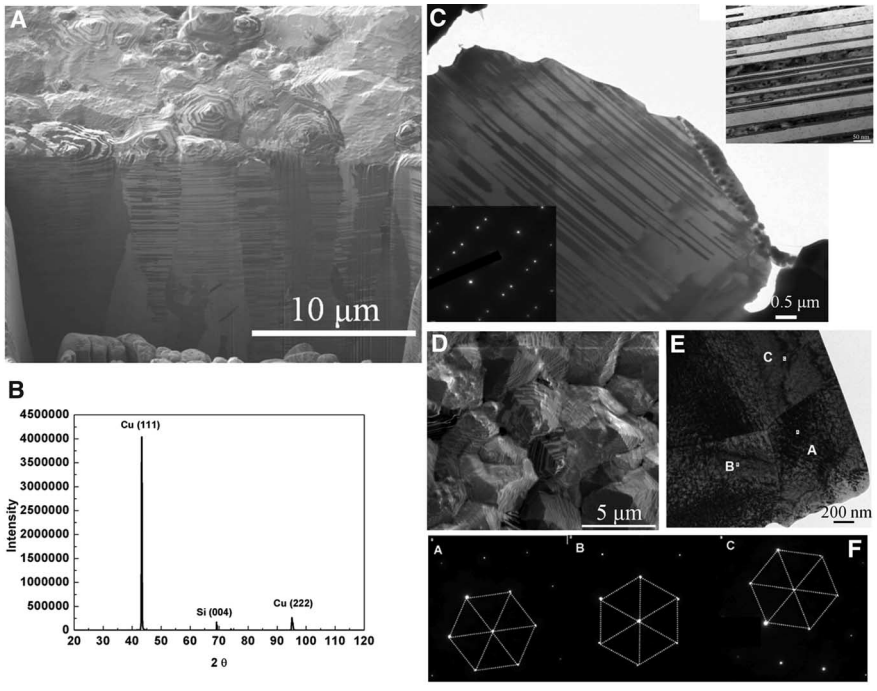

Fig. 1. The microstructural characterization of the electroplated Cu at a current density of 80 mA/cm^2 for 30 min at a stirring speed of 1200 rpm. (**A**) Cross-sectional FIB micrograph. (**B**) X-ray diffraction. (**C**) Cross-sectional image showing the Cu nanotwins near the cone. (**D**) Plan-view FIB micrograph. (**E**) Plan-view TEM image. (**F**) Diffraction patterns of the three grains in (E).

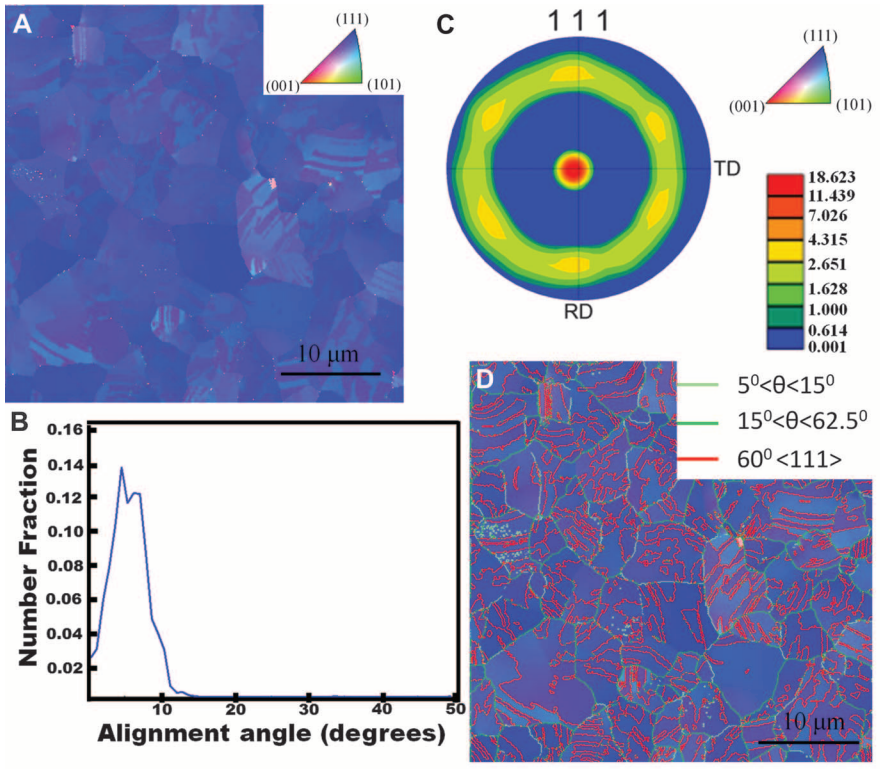

Fig. 2. EBSD analysis of the nt-Cu. (**A**) Plan-view inverse pole figure maps of the Cu surface. Color coding displays the out-of-plan direction in terms of the inverse pole figure. (**B**) Number fraction of the Cu grains deviated from [111] as a function of angle. (**C**) {111} pole figures of the fabricated Cu. TD and RD represent transverse direction and rolling direction, respectively. (**D**) Grain boundary characteristics.

reflow. Reflow means that the solder bump is melted to achieve chip-to-chip or chip-to-substrate joints. It is very difficult to control the solid-state microstructure as a molten solder bump solidifies; typically, the grains are randomly oriented. Furthermore, during the solid-state aging of the microbumps, the solder will transform into intermetallic compounds. These compounds will dominate the properties of the microbumps because the solder thickness decreases to about 10 μm or less in microbumps to connect the through-Si-vias (TSVs).

We report that using [111]-oriented nanotwinned Cu (nt-Cu) as the under-bump metallization promotes the unidirectional growth of intermetallic compounds in a large number of microbumps, leading to a uniform microstructure of all the microbumps. Unidirectional growth recalls the single-crystal turbine blades of a superalloy, requiring a crystal seed and a temperature gradient (*4*). To seed thousands of individual microbumps on a chip is impractical. Instead, we report a method of unidirectional growth that uses reactive epitaxial growth of

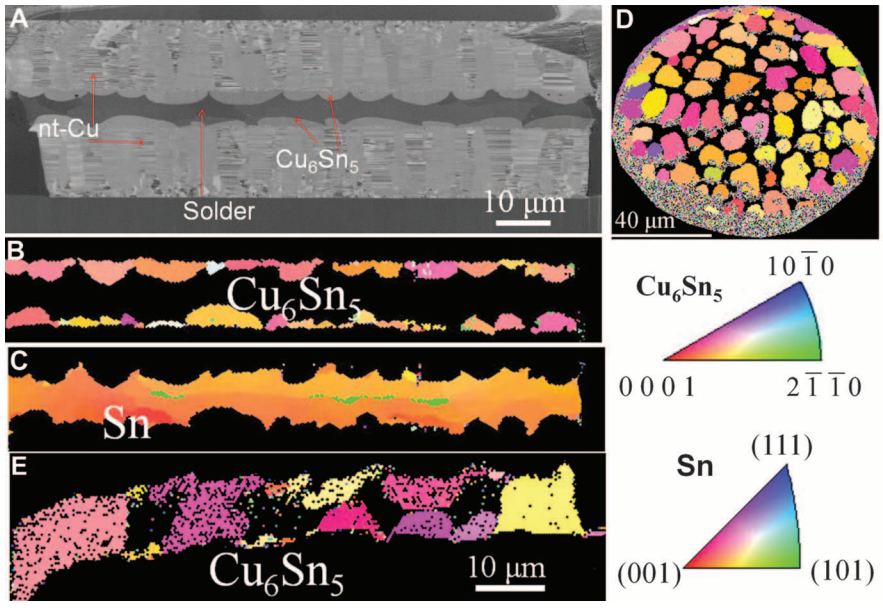

Fig. 3. (**A**) FIB image showing a microbump with 20-μm nt-Cu under-bump metallizations on both sides. (**B**) EBSD orientation image maps in the rolling direction for the Cu_6Sn_5 intermetallic compounds. (**C**) Orientation image maps for the remaining Sn2.5Ag in the rolling direction. (**D**) Plan-view orientation image maps in the normal direction for a microbump reflowed at 260°C for 5 min. (**E**) Another microbump reflowed for 5 min at 260°C.

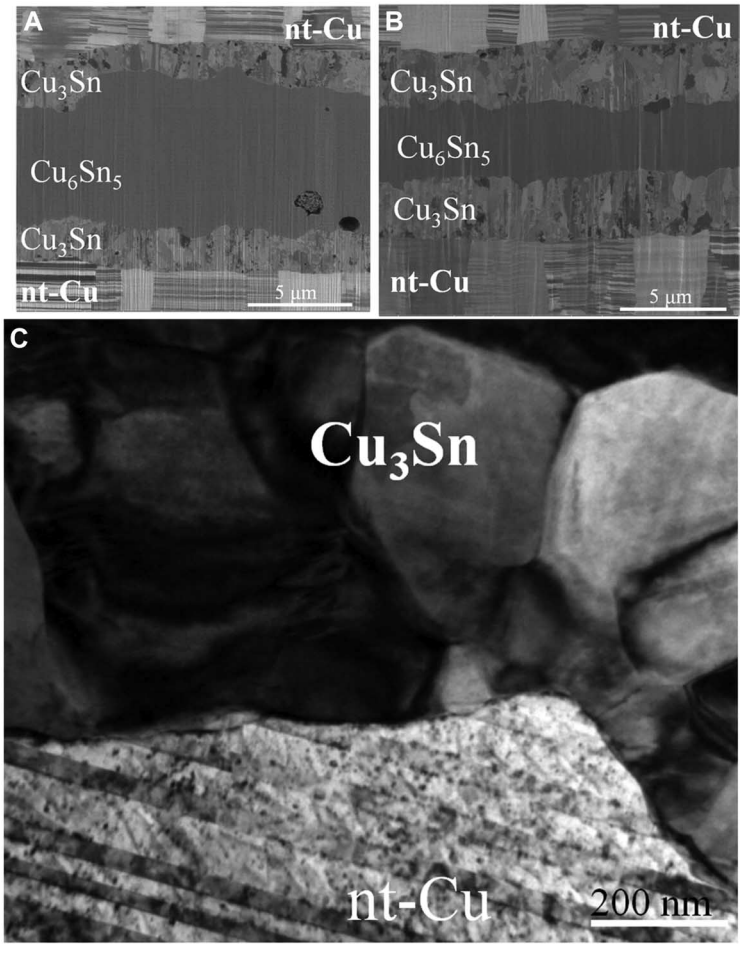

Fig. 4. Cross-sectional FIB image showing a microbump aged at 150°C (**A**) for 500 hours and (**B**) for 1000 hours. (**C**) Cross-sectional TEM image showing the interface of Cu_3Sn and nt-Cu.

microbumps on [111]-oriented nanotwin Cu. The [111] single crystals of Cu are replaced by [111]-oriented nt-Cu in every microbump. The small diameter of the microbump enables the growth of only a few oriented grains, and smaller and misoriented grains will be eliminated by ripening. The prerequisite is the preparation of oriented (111) nt-Cu as the under-bump metallization in each of thousands of microbumps. We have achieved this by introducing a rapid rotation of the electrolyte in the electroplating of Cu and by adding surfactants in the electrolyte solution.

Randomly oriented nt-Cu has been fabricated by using pulsed electroplating (*5*–*7*), and it possesses excellent mechanical strength (*8*–*11*). It also exhibits a higher electromigration resistance than regular Cu grains (*12*). For these reasons, nt-Cu has drawn a great deal of recent attention. Anderoglu *et al*. reported that nt-Cu with a [111] preferred orientation can be deposited via magnetron sputtering (*13*). However, in interconnect and packaging technology, Cu interconnects are deposited by electroplating.

In this report, [111]-oriented Cu grains with nt-Cu have been fabricated by dc electroplating with sulfuric acid as the electrolyte. Surfactants are added to the electrolyte, and the stirring speed of the electrolyte, ranging from 600 to 1200 revolutions per min (rpm), is critical to the outcome of the electroplating (*14*).

Highly oriented nt-Cu can be fabricated by specific current densities and stirring rates in electrolyte (supplementary materials and figs. S2 and S3). Figure 1A shows the cross-sectional focused ion beam (FIB) image for the nt-Cu electroplated with a current density of 80 mA/cm^2 at 1200 rpm for 30 min. The thickness of the Cu film is greater than 20 μm, and columnar Cu grains with unidirectional nanotwins are obtained (figs. S4 and S5). The normal of all the [111]-oriented nanotwins are aligned nearly parallel to the film growth direction. X-ray diffraction indicates that these Cu grains possess a very strong [111] preferred orientation (Fig. 1B and fig. S4). We note that many cones appear on the film surface. Spots from twins were observed in

the cross-sectional transmission electron microscopy (TEM) image and the corresponding electron diffraction pattern for the cone microstructure (Fig. 1C). The spacing of the nanotwins ranges from 10 to 100 nm. Figure 1D shows the plan-view FIB image of the cones on the Cu film surface. The nanotwins may have nucleated at the tips of the cones. The plan-view TEM and electron diffraction images of one of the cones have been examined to confirm the [111] orientation, and the edges of the cone exhibit sixfold symmetry. Figure 1E presents the plan-view TEM image for three neighboring (111) grains: A, B, and C in the middle of the sample, prepared by FIB polishing. The corresponding selected area diffraction pattern is shown in Fig. 1F. The rotation angle between grains A and B is 22°, whereas it is 15° between grains A and C.

Electron backscatter diffraction (EBSD) was used to analyze the statistical distributions of the grain orientations and the grain boundaries (fig. S1). The orientation image maps of the film surface after polishing by FIB show that the Cu film has a strong {111} texture (Fig. 2A). The corresponding color in the inverse pole figure (Fig. 2) represents the out-of-plane direction, indicating a very strong preferred orientation of [111]. The statistical data for the misalignment angles of the Cu (111) grains indicate that 96% of the columnar Cu grains have less than 10° of misalignment with respect to the [111] direction (Fig. 2B). In addition, Fig. 2C shows the fraction with the ⟨111⟩ out-of-plane direction in terms of the intensity of the central pole. The high density at the central pole reveals that a very high fraction of the electroplated Cu grains have a ⟨111⟩ preferred orientation. Figure 2D shows the grain boundaries, including the low, high, and twin boundaries. Here, we define low-angle grain boundaries as those with a misorientation angle less than 15° and high-angle boundaries as those with a misorientation angle between 15° and 65°. A twin boundary is categorized by a 60° angle grain boundary. The results indicate that most of the grain boundaries analyzed can be characterized as high-angle boundaries.

Suh reported the orientation relationship between a [001]-oriented Cu single crystal and the Cu_6Sn_5 grains (*15*). Zou studied the orientation relationships between the Cu_6Sn_5 grains and [111]-oriented Cu single crystals (*16*, *17*). We can fabricate oriented nt-Cu in patterned openings and have applied the very strongly oriented [111] nt-Cu to control the orientations of the Cu_6Sn_5 grains in a large number of microbumps (figs. S5 and S6). Figure 3A shows the cross-sectional FIB image of a microbump between two chips with a 10.5-μm-thick Sn2.5Ag solder after a reflow of 3 min at 260°C. The solder thickness is close to that found in 3D IC packaging. The Cu_6Sn_5 compounds grew on the (111) planes of the nt-Cu under-bump metallization. The EBSD orientation image maps for the Cu_6Sn_5 compounds indicate a preferred orientation near the (0001) plane of the Cu_6Sn_5 (Fig. 3B). Figure 3C presents the orientation image maps for the remaining Sn2.5Ag. A plan-view EBSD analysis was also performed to confirm the preferred orientation of all the Cu_6Sn_5 compounds on a microbump (Fig. 3D). Almost all the Cu_6Sn_5 grains have a preferred orientation close to (0001) (fig. S7). In another sample reflowed for 5 min at 260°C, some of the Cu_6Sn_5 grains on the top chip nearly touched the Cu_6Sn_5 grains on the bottom chip (Fig. 3E). Upon closer inspection, some have merged into one grain. We observe that two misoriented Cu_6Sn_5 grains on the top and bottom always merge into one single Cu_6Sn_5 grain, as indicated by the arrows in the figure.

Lastly, we note that the metallization on oriented nt-Cu forms very few or no Kirkendall (or Frenkel) voids during solid-state aging (*18*). It has been reported that severe Kirkendall voids form in the Cu_3Sn/Cu interface after solid-state aging in solder joints and greatly weaken the mechanical properties of the joint (*19*, *20*). The cross-sectional FIB image of a microbump after solid-state aging at 150°C for 500 hours (Fig. 4A) shows that the solder has been transformed completely into Cu_6Sn_5 and Cu_3Sn. The Cu_3Sn layer is 2.14 μm thick, yet only a few voids are observed in the Cu_3Sn/Cu interface. After aging at 150°C for 1000 hours, the Cu_3Sn layer thickness grew to 3.12 μm (Fig. 4B), and no obvious Kirkendall voids were found (fig. S8). Figure 4C shows the cross-sectional TEM image of the interface of Cu_3Sn/nt-Cu; some nanotwins end in Cu_3Sn grains. In transforming one molecule of Cu_6Sn_5 into two molecules of Cu_3Sn, the remaining three Sn atoms will attract nine Cu atoms to form three Cu_3Sn molecules, and the vacancies required for the Cu diffusion may condense to form voids. Although the twin boundaries are coherent, there are steps and kinks that can serve as vacancy sinks. In addition, Xu *et al*. reported that there are butt twins in the electroplated Cu and that they serve as vacancy sinks (*21*). The high density of nanotwins will provide high density of vacancy sinks. Therefore, no supersaturation of vacancies or nucleation of Kirkendall voids occurs. We expect that the electrical and mechanical properties of the microbumps without Kirkendall voids will be better.

Copper pillars without nanotwins have been implemented in microprocessors to increase the electromigration resistance and the performance of heat dissipation (*22*). The mechanically strong nanotwinned microbumps may cause a reliability concern because of chip-packaging interaction. In the traditional flip-chip technology, Si dies are bonded to polymer substrates, and large thermal stress thus occurs because of the mismatch in thermal expansion coefficients between the two materials. However, in 3D IC, Si dies are bonded to Si substrates of TSV interposers. Therefore, the chip-packaging interaction because of thermal stress is minimized in the microbumps.

By electroplating, we have fabricated highly oriented [111] nt-Cu in columnar [111]-oriented Cu grains in a large number of patterned under-bump metallizations of 20 μm diameter on Si wafers. The oriented nt-Cu can induce the unidirectional growth of [0001] Cu_6Sn_5 grains in solder reflow reactions. In subsequent solid-state aging, the nanotwin boundaries serve as vacancy sinks and prevent the supersaturation of vacancies at the interface of Cu_3Sn/Cu, leading to the formation of very few Kirkendall voids.

References and Notes

1. J. C. Lin *et al*., paper presented at IEEE International Electron Devices Meeting, San Francisco, CA, 6 December 2010.
2. M. Lu, D. Y. Shih, P. Lauro, C. Goldsmith, D. W. Henderson, *Appl. Phys. Lett.* **92**, 211909 (2008).
3. C. Chen, H. M. Tong, K. N. Tu, *Annu. Rev. Mater. Res.* **40**, 531 (2010).
4. D. R. Flack, *Fundamentals of Jet Propulsion with Applications* (Cambridge Univ. Press, New York, 2005), chap. 8.
5. L. Lu, Y. Shen, X. Chen, L. Qian, K. Lu, *Science* **304**, 422 (2004); 10.1126/science.1092905.
6. L. Lu, X. Chen, X. Huang, K. Lu, *Science* **323**, 607 (2009).
7. X. Li, Y. Wei, L. Lu, K. Lu, H. Gao, *Nature* **464**, 877 (2010).
8. J. Schiøtz, K. W. Jacobsen, *Science* **301**, 1357 (2003).
9. S. J. Zhou, D. L. Preston, P. S. Lomdahl, D. M. Beazley, *Science* **279**, 1525 (1998).
10. L. Lu, M. L. Sui, K. Lu, *Science* **287**, 1463 (2000).
11. K. Lu, L. Lu, S. Suresh, *Science* **324**, 349 (2009).
12. K. C. Chen, W. W. Wu, C. N. Liao, L. J. Chen, K. N. Tu, *Science* **321**, 1066 (2008).
13. O. Anderoglu *et al*., *Appl. Phys. Lett.* **93**, 083108 (2008).
14. See supplementary materials on *Science* Online.
15. J. O. Suh, K. N. Tu, N. Tamura, *J. Appl. Phys.* **102**, 063511 (2007).
16. H. F. Zou, H. J. Yang, Z. F. Zhang, *Acta Mater.* **56**, 2649 (2008).
17. H. F. Zou, H. J. Yang, Z. F. Zhang, *J. Appl. Phys.* **106**, 113512 (2009).
18. Y. Yin *et al*., *Science* **304**, 711 (2004).
19. K. Zeng *et al*., *J. Appl. Phys.* **97**, 024508 (2005).
20. R. Labie *et al*., paper presented at the 3rd Electronic System-Integration Technology Conference (IEEE Components, Packaging, and Manufacturing Technology Society), Berlin, Germany, 13 September 2010.
21. L. Xu *et al*., *J. Appl. Phys.* **104**, 113717 (2008).
22. A. Yeoh *et al*., paper presented at Electronic Components and Technology Conference (IEEE), San Diego, CA, 30 May 2006.

Acknowledgments: The financial support from the National Science Council, Taiwan, under the contract NSC 98-2221-E-009-036-MY3 is acknowledged. The authors thank J.-C. Kuo at National Cheng Kung University for assistance in the EBSD analysis. A patent, "Electrodeposited nano-twins copper layer and method of fabricating the same," is under application. The processing conditions of the (111)-oriented nt-Cu have been submitted for a patent application. The rest of the data and figures in this Report have not been presented or published elsewhere.

Supplementary Materials

www.sciencemag.org/cgi/content/full/336/6084/1007/DC1
Materials and Methods
Figs. S1 to S8

11 November 2011; accepted 19 April 2012
10.1126/science.1216511